Available online at www.sciencedirect.com

ScienceDirect

Geochimica et Cosmochimica Acta 156 (2015) 75–93

Geochimica et Cosmochimica Acta

www.elsevier.com/locate/gca

Experimental study of the replacement of calcite by calcium sulphates

E. Ruiz-Agudo [a,*], C.V. Putnis [b], J. Hövelmann [b], P. Álvarez-Lloret [c], A. Ibáñez-Velasco [a], A. Putnis [b]

[a] Department of Mineralogy and Petrology, University of Granada, Fuentenueva s/n, 18002 Granada, Spain
[b] Institut für Mineralogie, Universität Münster, Corrensstrasse 24, 48149 Münster, Germany
[c] Departmento de Geología, Universidad de Oviedo, c/ Jesús Arias de Velasco s/n, 33005 Oviedo, Spain

Received 16 October 2014; accepted in revised form 11 February 2015; available online 20 February 2015

Abstract

Among the most relevant mineral replacement reactions are those involving sulphates and carbonates, which have important geological and technological implications. Here it is shown experimentally that during the interaction of calcite ($CaCO_3$) cleavage surfaces with sulphate-bearing acidic solutions, calcite is ultimately replaced by gypsum ($CaSO_4$ $2H_2O$) and anhydrite ($CaSO_4$), depending on the reaction temperature. Observations suggest that this occurs most likely via an interface-coupled dissolution–precipitation reaction, in which the substrate is replaced pseudomorphically by the product. At 120 and 200 °C gypsum and/or bassanite ($CaSO_4{\cdot}0.5H_2O$) form as precursor phases for the thermodynamically stable anhydrite. Salinity promotes the formation of less hydrated precursor phases during the replacement of calcite by anhydrite. The reaction stops before equilibrium with respect to calcite is reached and during the course of the reaction most of the bulk solutions are undersaturated with respect to the precipitating phase(s). A mechanism consisting of the dissolution of small amounts of solid in a thin layer of fluid at the mineral–fluid interface and the subsequent precipitation of the product phase from this layer is in agreement with these observations. PHREEQC simulations performed in the framework of this mechanism highlight the relevance of transport and surface reaction kinetics on the volume change associated with the $CaCO_3$–$CaSO_4$ replacement. Under our experimental conditions, this reaction occurs with a positive volume change, which ultimately results in passivation of the unreacted substrate before calcite attains equilibrium with respect to the bulk solution.

1. INTRODUCTION

Mineral replacement reactions are relevant to all geochemical processes, including diagenesis, the redistribution of elements in the Earth's crust and hence the formation of many types of mineral and ore deposits (Ruiz-Agudo et al., 2014). When a solvent, such as water, is present, mineral replacement reactions may occur by the dissolution of the parent mineral and the precipitation of the replacing phase via an interface-coupled dissolution–precipitation mechanism (e.g. Putnis, 2002, 2009; Putnis and Putnis, 2007; Ruiz-Agudo et al., 2014). In these processes, an aqueous fluid induces some dissolution in the parent phase, resulting in an interfacial fluid layer supersaturated with respect to a more stable phase or phases. One or several of these phases may then nucleate onto the surface of the parent phase initiating an autocatalytic reaction that couples the dissolution and precipitation rate (Ruiz-Agudo et al., 2014 and Refs. therein). If there is a structural matching between the parent substrate and the product, epitaxial growth of the later on the former transfers crystallographic

* Corresponding author. Tel.: +34 958 240 473; fax: +34 958 243 368.
E-mail address: encaruiz@ugr.es (E. Ruiz-Agudo).

http://dx.doi.org/10.1016/j.gca.2015.02.012
0016-7037/

information from parent to product. These reactions are pseudomorphic, i.e. the external volume is preserved during the replacement. In order to propagate a pseudomorphic replacement front, the replacement product must be porous thus allowing continuous contact of the fluid phase with the unreacted surface of the parent phase. Volume changes in replacement are the result of both molar volume and relative solubility differences between parent and product (Putnis, 2002, 2009; Putnis and Putnis, 2007; Pollok et al., 2011; Ruiz-Agudo et al., 2014).

Among the most relevant mineral replacement reactions are those involving sulphates and carbonates, which have important geological and technological implications. For example, the transformation of evaporites to carbonates is a common diagenetic process. In particular, the carbonation of soluble minerals such as anhydrite ($CaSO_4$) and gypsum ($CaSO_4$ 2 H_2O) to give more stable carbonate phases has led to the formation of large deposits of diagenetic carbonates, as indicated by numerous authors (see Fernández-Díaz et al., 2009a,b and Refs. therein). The experimental works by Flörke and Flörke (1961), Fernández-Díaz et al. (2009a,b) and Roncal-Herrero et al. (2013) have focussed on the study of the microscopic mechanisms involved in the carbonation of gypsum. The inverse reaction, i.e. the sulphation of carbonates, is also a common process in nature and has important technological implications. Carbonate rocks are important building stone resources, and sulphation (gypsum crust formation) is one of the main causes responsible for carbonate stone (marbles, limestone and dolostone) deterioration in urban environments (e.g. Del Monte and Sabbioni, 1984; Vergés-Belmin, 1994; Booth et al., 1997). Furthermore, the replacement of calcite ($CaCO_3$) by gypsum is also relevant in the remediation of sulfate-bearing acid mine drainage, as calcite gravel is commonly used to retain metals and neutralize acidity, resulting frequently in the formation of gypsum (Hedin et al., 1994; Kleinmann et al., 1998; Cravotta and Trahan, 1999; Cravotta, 2003; Johnson and Hallberg, 2005). This wide range of applications has motivated several experimental studies aimed at improving the understanding of the calcite to gypsum transformation (e.g. Booth et al., 1997; Huminicki & Rimstidt, 2008; Hu et al., 2008; Atanassova et al., 2013; Offeddu et al., 2014). However, none of these studies have explored in detail the textural evolution and volume changes occurring during this transformation.

To our knowledge there are no studies aimed at elucidating the mechanism during the transformation of calcium carbonate into sulfate minerals under aqueous, hydrothermal conditions ($T > 100$ °C), i.e. those prevalent in subsurface environments. In these environments, the replacement of precursor carbonate minerals by silica, sulfide minerals or anhydrite can significantly modify the porosity and pore size distribution of carbonate rocks (Ahr, 2008) that are major oil, gas and groundwater reservoirs. The characteristics of the pore system of carbonate rocks strongly affect many technical and industrial aspects related to their exploitation as hydrocarbon reservoirs (Mazzullo and Chillingarian, 1992). Anhydrite ($CaSO_4$) is a frequent replacement mineral in carbonate reservoirs (Ahr, 2008) and, in fact, ca. 1 km below the surface anhydrite is the stable form of calcium sulfate (Hardie, 1967). Replacement of carbonates by anhydrite may occur during early diagenesis stages when sulfate-rich brines percolate downward through porous and permeable carbonate rocks and react with the minerals forming the rock (Ahr, 2008). Together with sulfate-rich brines, recent primary deposits of gypsum represent another source of sulfates for subsurface replacement of carbonates by anhydrite (Murray, 1964). Anhydrite may also form as a result of the interaction of carbonate rocks with upward-migrating fluids coming from deep-burial environments that invaded the reservoir from below (Ahr, 2008). Furthermore, anhydrite formation may occur during the injection of supercritical CO_2 into a deep saline aquifer for CO_2 geological sequestration. CO_2-rich, sulfate-bearing acid brines are produced that induce the dissolution of the carbonate minerals and the eventual precipitation of anhydrite (García-Rios et al., 2011). The formation of replacement anhydrite can dramatically reduce depositional porosity in carbonate reservoirs, which may have positive or negative consequences as reduced porosity due to anhydrite may prevent hydrocarbon leakage from the reservoir rocks (Ahr, 2008) but may also be detrimental for the CO_2 storage capability of the reservoirs.

Overall, a better knowledge of the mineralogical changes and the textural history of porosity during calcite–gypsum and calcite–anhydrite transformations may help to locate potential hydrocarbon reservoir rocks (Murray, 1964), as well as being relevant to remediation of acid mine drainage, building stone conservation, carbonate sedimentology, CO_2 geological sequestration and carbon and sulphur global cycling. This work is part of a broader study that deals with such transformations, with the ultimate goal of improving our understanding of the mechanisms controlling the replacement reactions involving carbonates and sulphates and the factors determining the porosity development during such processes. Here we focus on the study of the mineralogical and textural evolution, as well reaction pathways, while in a second paper (Ruiz-Agudo et al., submitted), we explore the crystallographic control and epitaxial relationships during $CaCO_3$–$CaSO_4$ transformations.

2. MATERIALS AND METHODS

2.1. Replacement reactions in Teflon® reactors

Small cleavage fragments (0.030 ± 0.005 mg weight, ca. $4 \times 3 \times 1$ mm in size) of optical quality calcite single crystals (Iceland spar) were reacted with 100 mM H_2SO_4 solutions (pH 1 at 22 °C). The experiments were conducted in tetrafluoroethylene-lined steel autoclaves (3 mL inner volume) held in an oven at 60, 120 and 200 ± 1 °C respectively for 1–288 h. Experiments conducted at 22 °C were treated in the same way as the oven experiments, but left in a temperature controlled room. Additional experiments were performed with a high concentration of background electrolyte (NaCl 4 M, high salinity experiments) with the aim of investigating its effect on the mineralogy of the precipitated phase. For each experiment 1.5 mL of solution was added

to the autoclave containing the crystal fragments that was then sealed and weighed. The oven was preheated to the required temperature before the autoclaves were placed inside. The samples were weighed at the end of the experiment after being cooled in air to ensure that no fluid had been lost.

2.2. Analysis of solids and solution after the reactions

After the experiments the crystals were removed from the solution, washed with ethanol, and dried. Solutions were analyzed for Ca and S using ICP-OES, and pH was measured using a micro combination electrode model PHR-146B (Lazar Laboratories). Total dissolved inorganic carbon (dissolved CO_2, bicarbonate and carbonate ions) in the solution was measured immediately after the reaction using a CO_2-selective electrode coupled to a Methrohm pH meter. Nevertheless, these measurements failed to provide the total concentration of C-bearing species due to CO_2 degassing at low pH conditions once the reactors were opened at room temperature after the reaction, and total inorganic carbon was finally calculated by mass-balance. Selected experiments were repeated three times to determine errors in the concentration measurements, which were found to vary between 1 and 10%. This is not surprising as the reactive surface area of the crystals may vary significantly, although the weight of the crystals in the reactor was kept similar in all the experiments. Experimental conditions, pH and the corresponding Ca, S and TIC concentrations in solution after the experiments are summarized in Table 1.

For phase identification crystal surfaces were analyzed by X-ray diffraction (XRD). In order to maximize the signal from the thin surface layer of the precipitate and minimize the penetration depth of the X-rays into the calcite substrate, data were obtained in grazing incident angle mode (GIAXRD), by carrying out scans at a fixed small incident angle of the X-ray beam on the substrate surface. Analysis conditions were: radiation Cu Kα (λ:1.5405 Å), 45 kV voltage, 40 mA current intensity, and goniometer speed of 0.01° 2θ/s using Si-detector X'Celerator. The grazing angle (ω) was 2° and the investigated area between 5° and 60° 2θ.

2.3. Textural characterization and microRaman analysis of reacted solids

A JEOL 6300F Field Emission Scanning Electron Microscope (FESEM) equipped with a back-scattered electron (BSE) and energy-dispersive X-ray (EDX) detector was used for texture examinations. Partially replaced crystals were embedded into epoxy resin blocks and polished using a non-aqueous fluid (decane). Selected samples were then carbon coated and examined by FESEM in backscattered electron mode using a 20 keV beam.

A confocal Raman spectrometer (Horiba Jobin Yvon XploRA) operating with the 638 nm line of a He–Ne laser was used for spatially resolved identification of phases in the reaction rim. The scattered light was collected in a 180° backscattering geometry and analyzed with a charge-coupled device (CCD) detector after being dispersed by a grating of 1200 grooves/mm and passed through a 100 μm entrance slit. All spectra were collected using a 100× objective, a confocal aperture of 500 μm and an acquisition time of 3 × 15 s. Corrections for system drift were done using the 520.7 nm Raman band of a silicon standard taken at the beginning and the end of each measuring session.

2.4. Modelling of the evolution of solution composition

Activities of different relevant chemical species in the system and supersaturation with respect to possible $CaSO_4$ phases were calculated using PHREEQC (Parkhurst & Appelo, 1999). The saturation index is defined as

$$\mathrm{SI} = \log \Omega = \log \frac{\mathrm{IAP}}{K_{sp}} = \log \frac{a_{Ca^{2+}} \cdot a_{SO_4^{2-}}}{K_{sp}} \quad (1)$$

where Ω is the supersaturation, IAP is the ion activity product, $a_{Ca^{2+}}$ and $a_{SO_4^{2-}}$ are the calcium and sulphate activities in solution, and K_{sp} is the solubility product of the phase considered. The input parameters for these calculations are ion concentrations and pH values measured (see Section 2.2).

3. RESULTS

3.1. Mineralogical evolution during the $CaCO_3$–$CaSO_4$ transformation

SEM observations, EDX and micro-Raman analysis of cross-sections of partially reacted samples show that during the interaction of sulphate-bearing acidic solutions and Iceland spar fragments, calcite is pseudomorphically replaced by calcium sulphate(s) (Figs. 1–4). The mineralogy of the phases precipitated under the different experimental conditions, determined by GIAXRD, is shown in Fig. 5 and summarized in Table 2. At room temperature, gypsum was already detected after 1 h of reaction in the replacement rim, and no other different phases were found at longer reaction times. The same applies for $T = 60$ °C. Interestingly, in the reactions performed in low salinity environments ([NaCl] = 0) at 120 °C, gypsum was observed to precipitate at short reaction times ($t = 1$ h) at together with bassanite, but after 1 day of reaction only bassanite was identified in the XRD pattern, and at $t \geqslant 120$ h the product was exclusively anhydrite. When high salinity ([NaCl] = 4 M) solutions were used no gypsum was detected. At 200 °C (both in low and high salinity solutions), bassanite was found at short reaction times (1 h), and anhydrite was the only phase detected at $t \geqslant 24$ h.

According to the results of the Raman analysis, the reaction products can be identified as gypsum, bassanite and/or anhydrite, depending on the temperature and the time of reaction. As discussed below, the change in Raman shift of the $\nu_1(SO_4)$ band with respect to varying hydration states, can be utilized to distinguish between various hydrated forms of $CaSO_4$. This identification is also supported by differences in the shift and number of the ν(OH) bands.

In our samples, the $\nu_1(SO_4)$ mode in gypsum (identified in the replacement rim of samples reacted at 22 °C and 60 °C (any reaction time) and at 120 °C during 1 h,

Table 1
Experimental conditions (Temperature, T, and reaction time, t) and compositional data (pH, calcium, sulfate and dissolved inorganic carbon (DIC) concentrations), as well as calculated calcium ($a_{Ca^{+2}}$) and sulfate ($a_{SO_4^{-2}}$) activities and saturation indexes (SI) with respect to calcite, gypsum, bassanite and anhydrite.

T (°C)	[NaCl] (M)	t (h)	[Ca] (mM)	[SO_4] (mM)	[DIC] (mM)	pH	$\log a_{Ca^{+2}}$	$\log a_{SO_4^{-2}}$	$SI_{calcite}$	SI_{gypsum}	$SI_{anhydrite}$	$SI_{bassanite}$
25	0	0	0.00	100.00	0.00	1.10	–	–	–	–	–	–
25	0	1	14.66	73.26	41.40	1.27	−2.47	−2.15	−9.51	−0.09	−0.27	−0.91
25	0	24	11.08	65.88	45.20	1.29	−2.58	−2.17	−9.55	−0.22	−0.40	−1.04
25	0	120	11.10	59.99	51.11	1.33	−2.57	−2.18	−9.39	−0.21	−0.39	−1.03
25	0	288	15.75	41.28	74.47	1.60	−2.39	−2.19	−8.51	−0.05	−0.23	−0.87
25	4	0	0.00	100.00	0.00	1.15	–	–	–	–	–	–
25	4	1	34.38	75.36	59.02	1.24	−2.30	−2.91	−9.30	−0.68	−0.86	−1.50
25	4	24	28.92	47.46	81.46	1.56	−2.36	−3.07	−8.59	−0.90	−1.08	−1.72
25	4	120	29.00	44.66	84.34	1.63	−2.36	−3.09	−8.43	−0.92	−1.10	−1.74
25	4	288	24.39	31.04	93.35	1.99	−2.43	−3.23	−7.74	−1.13	−1.31	−1.95
60	0	0	0.00	100.00	0.00	1.10	–	–	–	–	–	–
60	0	1	9.47	57.15	52.32	1.41	−2.58	−2.44	−8.62	−0.39	−0.24	−0.89
60	0	24	15.94	55.23	60.71	1.52	−2.38	−2.39	−8.12	−0.13	0.02	−0.63
60	0	120	13.16	39.66	73.50	1.67	−2.42	−2.41	−7.78	−0.20	−0.05	−0.70
60	0	288	8.43	18.26	90.17	2.04	−2.54	−2.48	−7.06	−0.39	−0.24	−0.89
60	0	0	0.00	100.00	0.00	1.15			–	–	–	–
60	4	1	24.62	55.32	69.30	1.37	−2.50	−3.11	−8.54	−0.98	−0.83	−1.48
60	4	24	29.91	60.64	69.27	1.38	−2.41	−3.07	−8.43	−0.85	−0.70	−1.35
60	4	120	33.09	59.51	73.58	1.45	−2.37	−3.06	−8.23	−0.80	−0.65	−1.30
60	4	288	30.77	50.86	79.91	1.55	−2.40	−3.10	−8.01	−0.87	−0.72	−1.37
120	0	0	0.00	100.00	0.00	1.10	–	–	–	–	–	–
120	0	1	12.67	50.38	62.28	1.62	−2.44	−2.79	−7.15	−0.18	0.45	−0.21
120	0	24	19.77	38.80	80.96	2.06	−2.28	−2.57	−6.00	0.20	0.83	0.17
120	0	120	15.14	17.42	97.72	3.04	−2.38	−2.44	−4.06	0.23	0.86	0.20
120	0	288	25.11	29.12	95.99	2.91	−2.25	−2.32	−4.18	0.48	1.11	0.45
120	4	0	0.00	100.00	0.00	1.15	–	–	–	–	–	–
120	4	1	29.85	58.46	71.39	1.35	−2.93	−3.45	−8.24	−0.18	0.45	−0.21
120	4	24	22.61	32.75	89.86	1.66	−2.73	−3.41	−7.30	0.20	0.83	0.17
120	4	120	18.53	21.87	96.66	2.51	−2.84	−3.57	−5.62	0.23	0.86	0.20
120	4	288	4.22	12.72	91.51	2.35	−2.63	−3.37	−5.74	0.48	1.11	0.45
200	0	0	0.00	100.00	0.00	1.10	–	–	–	–	–	–
200	0	1	22.46	57.94	64.52	1.88	−2.34	−3.00	−5.74	0.80	1.95	1.26
200	0	24	5.04	37.98	67.06	1.66	−2.85	−3.35	−6.67	−0.06	1.09	0.40
200	0	120	4.96	26.05	78.91	1.86	−2.79	−3.30	−6.14	0.05	1.20	0.51
200	0	288	4.53	22.37	82.16	1.93	−2.82	−3.30	−6.01	0.02	1.17	0.48
200	4	0	0.00	100.00	0.00	1.15	–	–	–	–	–	–
200	4	1	33.66	70.21	63.46	1.59	−2.78	−3.62	−6.81	−0.26	0.89	0.20
200	4	24	18.37	40.14	78.23	1.72	−3.04	−3.78	−6.71	−0.68	0.47	−0.22
200	4	120	9.68	23.53	86.14	1.84	−3.31	−3.95	−6.71	−1.12	0.03	−0.66
200	4	288	13.20	21.31	91.90	2.10	−3.18	−3.89	−6.03	−0.93	0.22	−0.47

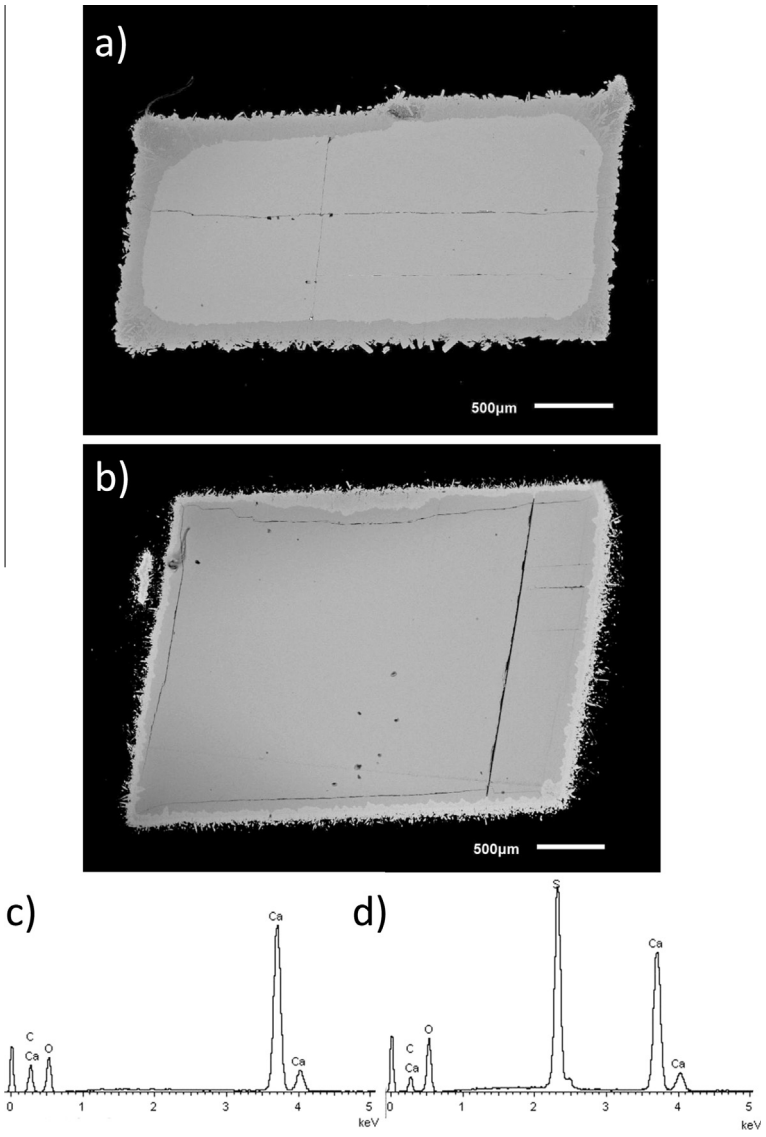

Fig. 1. (a) Gypsum and (b) anhydrite pseudomorphs formed after the reaction of calcite fragments with a 100 mM H_2SO_4 solution at 60 °C during 288 h and 200 °C during 120 h, respectively. Representative EDX analysis of (c) unreacted core and (d) reaction rim.

Figs. 2 and 6c, d) is centered at 1011 cm^{-1} and shifts to higher wavenumbers (1016 and 1018 cm^{-1}) with the lower water content of bassanite (identified in samples reacted at 120 °C during 1 h and 24 h, and at 200 °C during 1 h, Figs. 6 and 7c, d) and anhydrite (identified in samples reacted at 120 and 200 °C during 24, 120 and 288 h, Figs. 6 and 7c, d). This shift is related with the fact that the S–O bond in anhydrite and bassanite is stronger (and shorter) than in gypsum, and that there is an inverse relationship between bond length and its Raman shift (Chio et al., 2004). Note that in Fig. 6c, the shape of the $v_1(SO_4)$ band located at 1016 cm^{-1} is asymmetric, which suggests that a small amount of gypsum may be present. The small shoulder causing this asymmetry in the band would be related with the presence of the $v_1(SO_4)$ band in gypsum located at 1011 cm^{-1} (Chio et al., 2004). The $v_3(SO_4)$ mode which appeared at around 1139 cm^{-1} in gypsum disappears in bassanite and splits into two peaks at around 1130 and 1163 cm^{-1} in anhydrite. Additionally, two new vibration modes appear in anhydrite: a band around 1088 cm^{-1} and a broad band located at 1115 cm^{-1}.

Besides the shift in the SO_4-stretching modes, the different $CaSO_4$ phases can be also identified by the displacement of the OH-stretching bands (Chio et al., 2004). In the gypsum spectra there are two strong bands centered at 3400 and 3500 cm^{-1}. The first one belongs to the $v_1(H_2O)$ mode and the second one to the $v_3(H_2O)$ mode. This is so due to the asymmetric geometry of the water molecules in gypsum. The shorter OH_2 bond locates at a higher wavenumber than the longer OH_1 bond. In bassanite, these bands shift to higher wavenumbers (3556 and 3616 cm^{-1}) in agreement with the significant increase in the O(water)···O(sulfate) bonding distance with respect to gypsum (Chio et al., 2004). In anhydrite, these bands disappear (Chio et al., 2004). All these features described above permit unambiguous, space-resolved identification of replacement $CaSO_4$

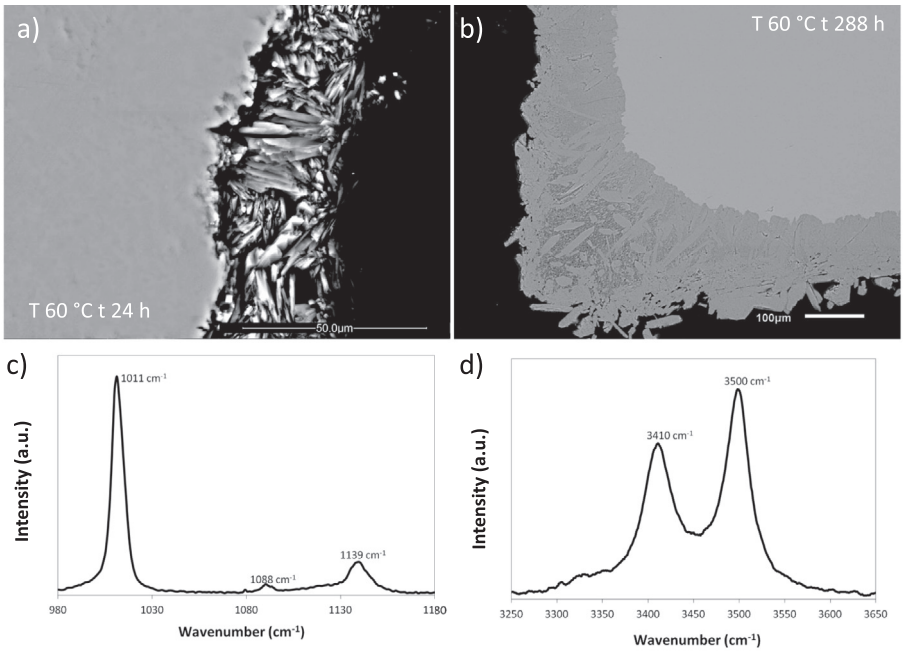

Fig. 2. BSE images and microRaman spectra of cross-sections of calcite crystals partially replaced by gypsum in a 100 mM H_2SO_4 solution (pH 1). (a) Porous rim formed by coarse gypsum crystals (60 °C, 24 h). (b) Thick gypsum crystals inlaid within a fine-grained, nanocrystalline matrix (60 °C, 288 h). (c, d) Representative Raman spectra of the replacement rim in the 980–1180 cm^{-1} and 3250–3650 cm^{-1} region, respectively.

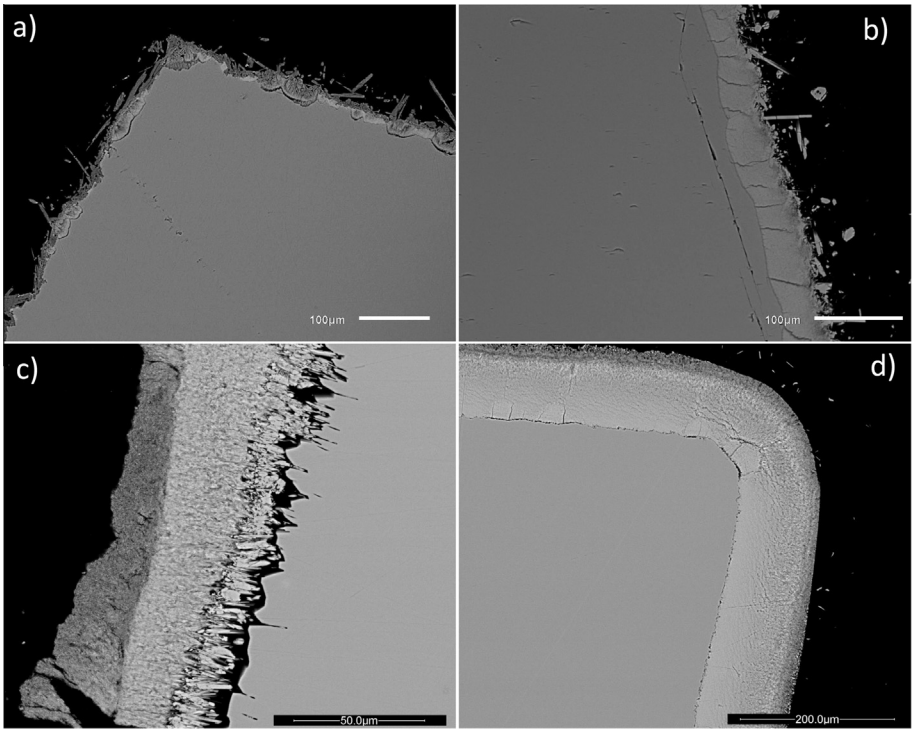

Fig. 3. BSE images of cross-section of partially replaced crystals showing the different stages in the replacement of calcite by $CaSO_4$ at T 120 °C in a 100 mM H_2SO_4 solution (pH 1). (a) Coexistence of bassanite (fine grained crystals, inner porous rim) and gypsum (coarser crystals, outer porous rim) at $t = 1$ h. (b) Porous rim formed by coarse anhydrite crystals (outer layer) at $t = 24$ h. (c) Anhydrite rim with coarse texture close to the unreacted calcite core and fine-grained, porous texture in the outermost part. (d) Compact, homogeneous rim of anhydrite with decreasing porosity towards the calcite substrate ($t \geqslant 120$ h).

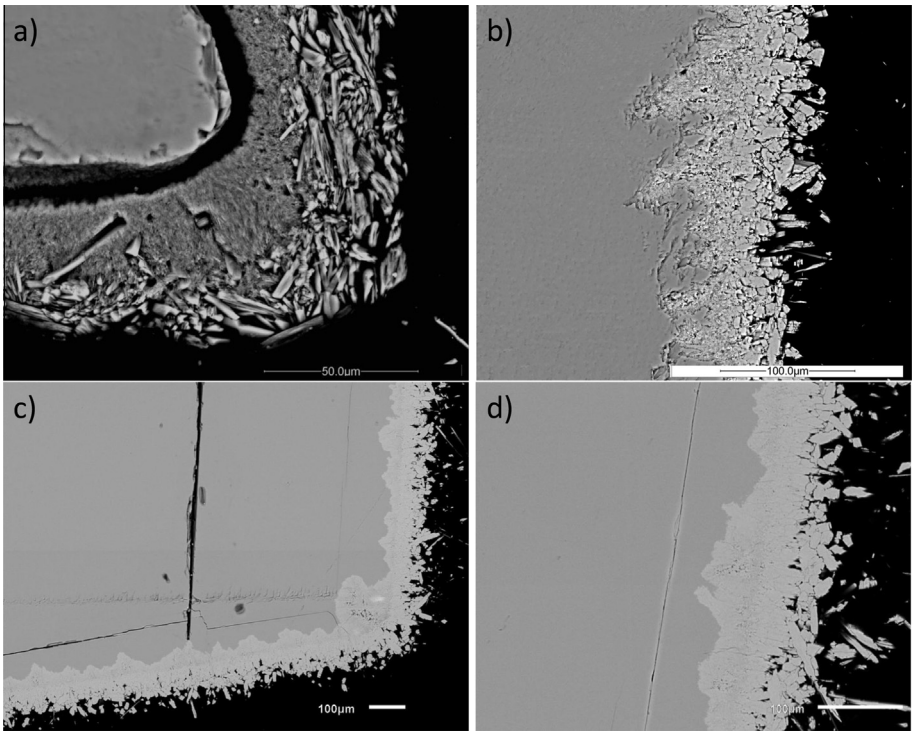

Fig. 4. BSE images of cross-section of partially replaced crystals showing the different stages in the replacement of calcite by $CaSO_4$ at T 200 °C in a 100 mM H_2SO_4 solution (pH 1). (a) Bassanite rim formed at $t = 1$ h. Two different porous textures are visible: fine grained crystals, inner porous rim and coarse crystals, outer porous rim at $t = 1$ h. (b) Porous rim formed by coarse anhydrite crystals at $t = 24$ h. (c, d) Compact, homogeneous rim of anhydrite with decreasing porosity towards the calcite substrate ($t \geqslant 120$ h).

phases using micro-Raman spectroscopy (supported by XRD data), and allow determining the reaction mechanisms and pathways described in the discussion section.

3.2. Evolution of solution chemistry

Table 1 and Fig. 8 show the evolution of the DIC, sulphate and calcium concentration and pH of the aqueous solution during the interaction of sulphate-bearing acidic solutions with the calcite. In all the experiments performed, the sulphate content of the solution decreases with reaction time, while DIC concentration increases. Overall, calcium concentration does not show significant variations with reaction time, i.e. it is somehow "buffered" by the reactions taking place in the system. In general, sulphate and DIC concentrations seem to have reached an asymptotic value after 288 h of reaction, i.e. the system reaches an equilibrium at the end of the experiments.

Calcium, sulphate and DIC concentrations show complex trends with temperature and salinity. Increasing reaction temperature results in a decrease in the sulphate concentrations measured after the reaction, with no significant changes observed at $T \geqslant 120$ °C. For $T \leqslant 120$ °C, DIC concentrations are higher at higher temperatures. However, at 200 °C DIC concentrations are lower than those measured at 120 °C. Calcium concentrations are very similar at 22 °C, 60 °C and 120 °C, decreasing slightly upon increasing the temperature up to 200 °C. In general, calcium concentrations seem to increase with salinity, this being particularly evident at the lowest temperatures tested here. At 22 and 60 °C, DIC increases with salinity (i.e. more calcite is dissolved); the same is observed at 200 °C. However, at 120 °C an increase in salinity does not result in significant changes in [DIC] (i.e. similar amount of calcite dissolved). Sulphate concentrations do not seem to be significantly affected by an increase in salinity at T 120 and 200 °C. At 22 °C and 60 °C, opposite behaviour is found: in the first case, increasing salinity results in decreasing sulphate concentration and in the second case, increasing salinity leads to higher sulphate in solution.

3.3. Driving force for the replacement process

To determine the driving forces during the experiments, the activities of aqueous species as well as saturation indexes with respect to the different Ca-bearing phases relevant to the system have been calculated from experimentally measured data using PHREEQC and the llnl.dat database (Parkhurst & Appelo, 1999), also used in Ossorio et al. (2014). All solutions were found to be highly undersaturated with respect to calcite at all reaction times (Table 1). Increasing the reaction temperature to 120 °C, SI_{Cc} was found to increase (i.e. SI_{Cc} is less negative or, in other words, the solution is closer to equilibrium with respect to calcite), both at low and high salinity. Interestingly, on a further increase of temperature up to 200 °C, SI_{Cc} decreases (i.e. SI_{Cc} is more negative or, in other words, the solution is more undersaturated with respect to calcite).

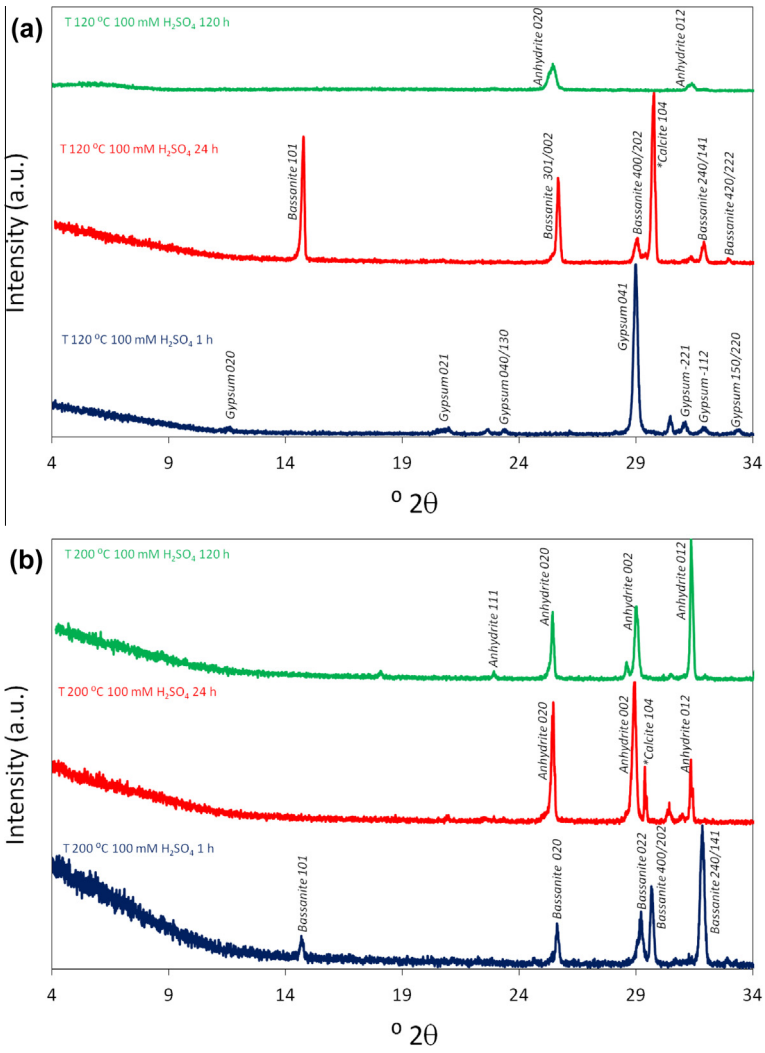

Fig. 5. Mineralogical evolution during the $CaCO_3$ to $CaSO_4$ transformation determined by XRD as a function of temperature (T), time (t) and salinity. XRD patterns at 25 °C and 60 °C are not displayed as were found to be gypsum regardless of the reaction time.

Table 2
Mineralogical evolution during the $CaCO_3$ to $CaSO_4$ transformation, as a function of temperature (T), time (t) and salinity. Black filling: gypsum; dark grey filling: bassanite; light grey filling: anhydrite.

	t (h)			
	NaCl 0 M			
T (ºC)	**1**	**24**	**120**	**288**
22				
60				
120				
200				
	NaCl 4 M			
T (ºC)	**1**	**24**	**120**	**288**
22				
60				
120				
200				

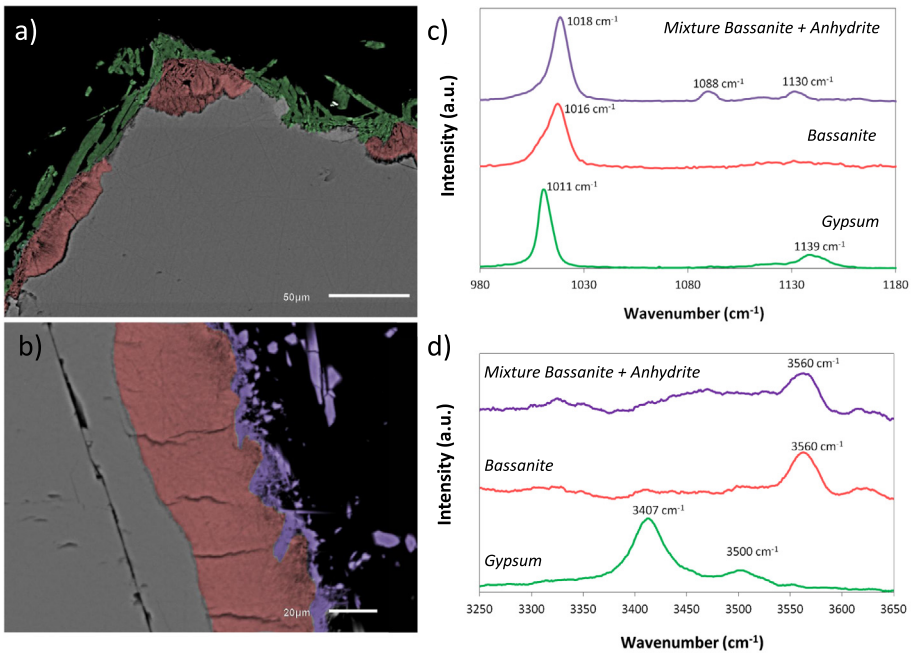

Fig. 6. (a, b) BSE images of cross-section of partially replaced crystals at T 120 °C in a 100 mM H_2SO_4 solution (pH 1) and (c, d) the corresponding Raman spectra. False color in BSE images corresponds to the line colors in the Raman spectra. (For interpretation of the references to colour in this figure legend, the reader is referred to the web version of this article.)

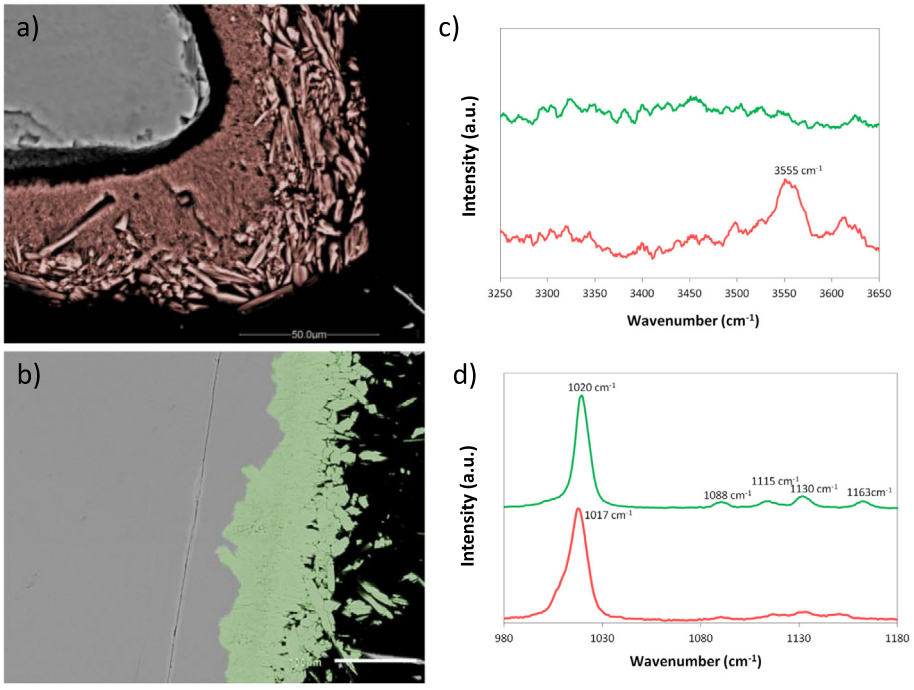

Fig. 7. BSE images of cross-section of partially replaced crystals at T 200 °C in a 100 mM H_2SO_4 solution (pH 1) and the corresponding Raman spectra. False color in BSE images corresponds to the line colors in the Raman spectra. (For interpretation of the references to colour in this figure legend, the reader is referred to the web version of this article.)

Regarding calcium sulphate phases, at 22 °C and 60 °C the solutions were undersaturated or at equilibrium with respect to the thermodynamically stable phase (i.e. gypsum at 22 °C and anhydrite at 60 °C) (Fig. 9). Note that anhydrite was not identified in the reaction product at these temperatures, and only gypsum was found in the replacement product. Under high salinity conditions, the solutions were undersaturated with respect to any calcium sulphate

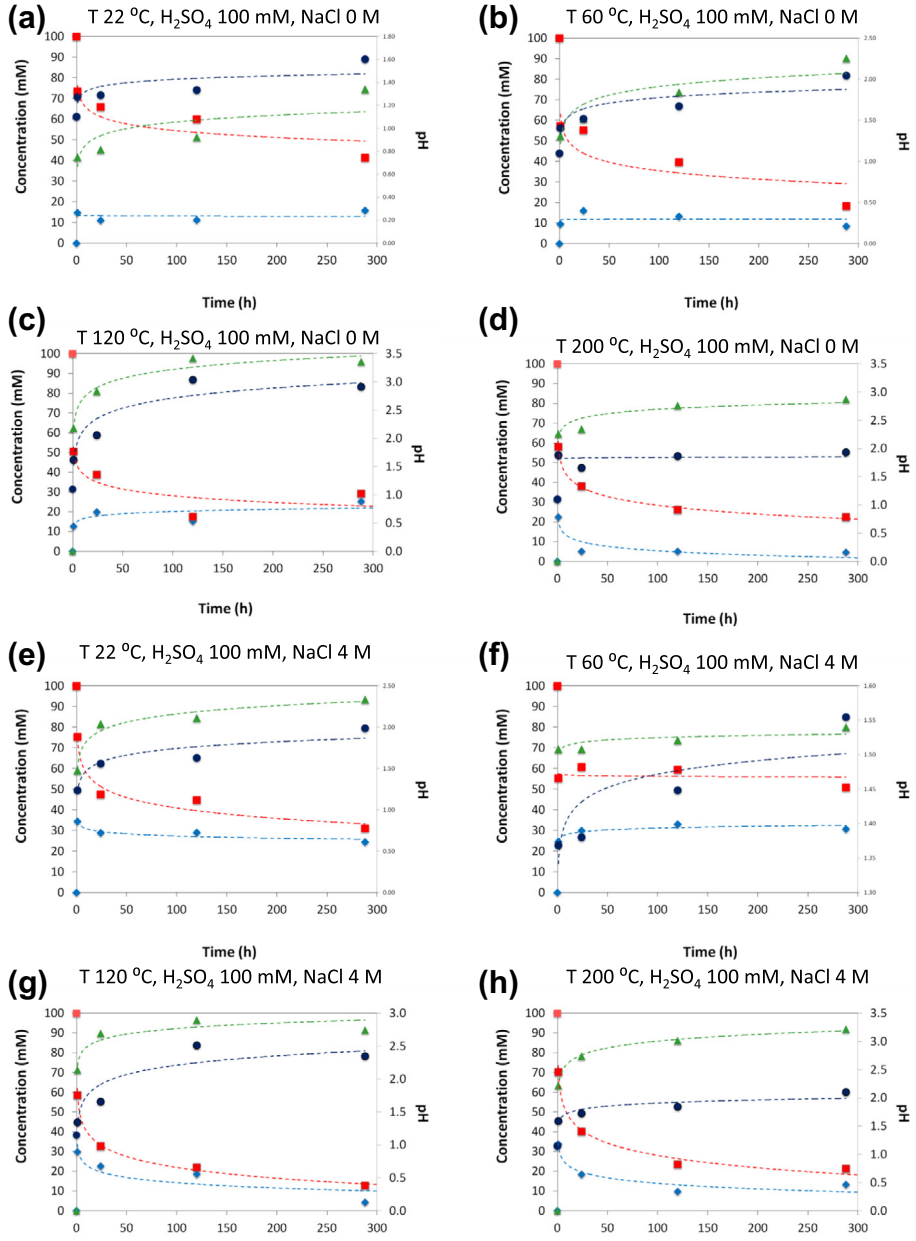

Fig. 8. Evolution of solution composition as a function of reaction time, for different temperatures and salinities. pH = dark blue line; calcium concentration = light blue line; sulfate concentration = red line and dissolved inorganic carbon (DIC) concentration = green line. (For interpretation of the references to colour in this figure legend, the reader is referred to the web version of this article.)

phase, although the formation of gypsum was also detected at $t \geqslant 1$ h. At 200 °C, virtually all solutions were found to be undersaturated with respect to any calcium sulphate phase regardless of the salinity (Table 1 and Fig. 9), despite the fact that bassanite was found to precipitate after 1 h of reaction, as indicated by the XRD analyses and the measured decrease in the sulphate content of the solution. Only after 288 h of reaction and at low salinity, the solution becomes supersaturated with respect to anhydrite, but remains undersaturated with respect to bassanite and gypsum. The same is true for 120 °C and high salinity, whereas at low salinity the solution after 1 h of reaction is at equilibrium with respect to anhydrite, becomes progressively supersaturated with respect to anhydrite and is at equilibrium with respect to bassanite and gypsum after 288 h of reaction (Table 1 and Fig. 9).

3.4. Textural evolution and micro-Raman characterization of partially reacted crystals

As stated before, our experimental observations indicate that upon interaction with sulphate-bearing acidic solutions, calcite is pseudomorphically replaced by calcium sulphate(s). Fig. 10 shows the thickness of the transformed

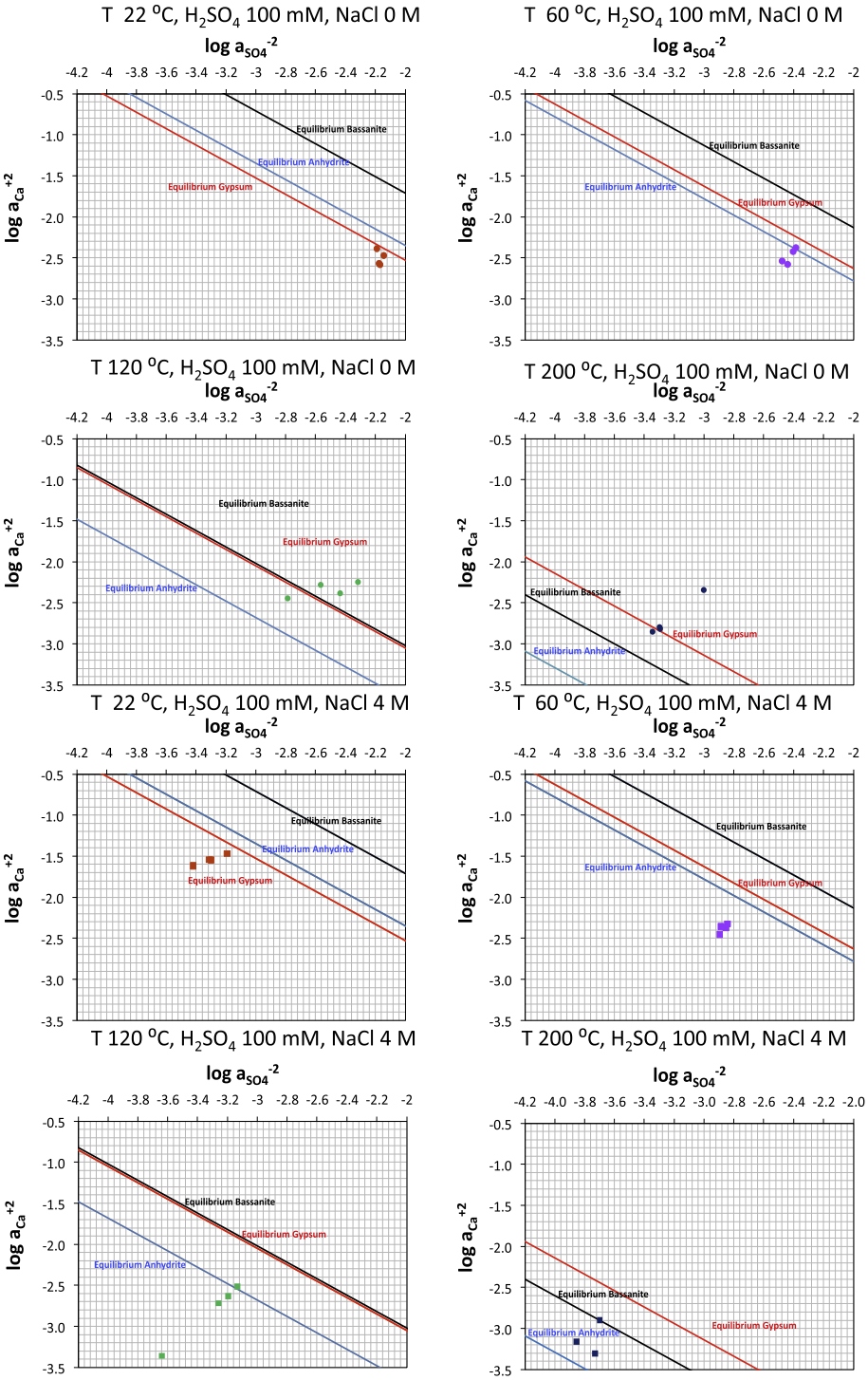

Fig. 9. Equilibrium diagrams and calculated activity data for different reaction temperatures and salinities.

layer as a function of time, for different temperatures and NaCl = 0 M (lines are just given as a guide for the eyes). No attempt was made to fit the experimental data to any kinetic equation due to the lack of a significant number of measurements for each experimental point. However, this figure gives interesting insights into the mechanism of the replacement reaction and, particularly, the formation of passivation layers. For the lower temperatures tested (22 °C and 60 °C) a sigmoidal-type of behaviour is observed, which is not seen at higher temperatures. This is interpreted as a slow, almost linear advancement of the replacement front in the initial stages of the replacement, which is slowly retarded with increasing reaction time. At 120 °C and 200 °C, the width of the calcium sulphate layer rapidly increases with time during the early stages of the process; however, this is quickly followed by a second stage

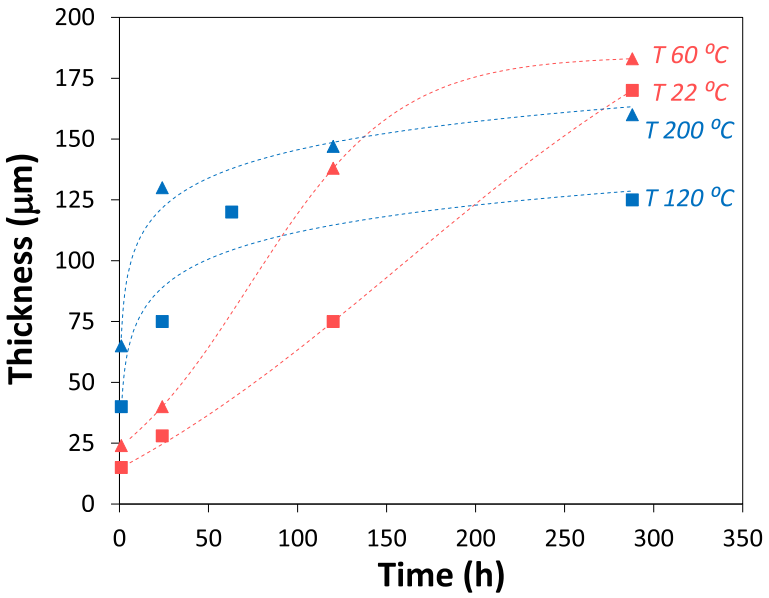

Fig. 10. Thickness of the reaction rim during the $CaCO_3$–$CaSO_4$ transformation as a function of time and reaction temperature (NaCl = 0 M). Lines are plotted as a guide for the eye.

in which the advance of the replacement front completely ceases.

At 22 °C and 60 °C, partially replaced crystals show very similar features (Fig. 2a, b). A replacement rim is clearly seen already after 1 h of reaction, which increases in thickness with reaction time. This rim is identified to be $CaSO_4$ by EDX, and appears darker than the inner core of unreacted calcite in BSE images. The rim is formed initially by large, thick calcium sulphate crystals with a large intercrystalline porosity. With increasing reaction time, these thick crystals appear inlaid within a matrix of fine-grained, nanocrystalline texture, whose porosity seems to decrease during the advancement of the reaction. The Raman spectrum of the replacement rim does not change with the position in the replacement rim or the reaction time (Fig. 2c, d) and indicate that gypsum is the phase formed under these conditions.

After 1 h of reaction at 120 °C, two different textures were found in the replacement rim (of average thickness ca. 40 μm) (Figs. 3 and 6a). The outer part of the replacement rim is formed by large, thick crystals of thickness ranging from 1 to 6 μm. An inner, highly porous layer formed by nanocrystallites is observed closer to the unreacted core of calcite. Both layers were found to be $CaSO_4$ by EDX; however, they show slightly different contrast in BSE images (the outer part appears darker than the unreacted calcite, will the inner rim appears lighter) and significantly different Raman spectra (Fig. 6). According to the Raman results, the outer layer is formed by gypsum while the inner layer is formed by bassanite. After 24 h of reaction, the darker outer gypsum rim is not present. The same (apparently) nanocrystalline layer observed at shorter reaction times in contact with the unreacted substrate appears thicker, less porous and homogeneously distributed on the calcite surface (Figs. 3 and 6b). Cracks perpendicular to the calcite surface appear more or less regularly spaced within this layer. On top of this layer, a thin layer of coarser crystals is observed. Again, both layers were found to be $CaSO_4$ by EDX but they show slightly different contrast in BSE images (both of them lighter than the calcite substrate, and the outer rim lighter than the inner one) and significantly different Raman spectra (Fig. 6). The outer layer was found to be anhydrite while the inner layer is bassanite again. At longer reaction times ($t \geqslant 120$ h), a continuous rim with coarse texture close to the unreacted calcite core and fine-grained, porous texture in the outermost part is observed (Fig. 3c). With increasing reaction time, the rim appears more compact and homogeneous with decreasing porosity towards the calcite substrate (Fig. 3d). Differences in BSE contrast in this case seem to be related to differences in porosity, as the Raman spectra from inner and outer parts of the replacement rim do not show significant differences and are consistent with that of anhydrite, and it is similar to the spectra from the outer layer observed at 24 h.

At 200 °C, a ca. 65 μm thick rim is already formed after 1 h of reaction. Again, two different textures were found in the replacement rim (Figs. 4, 7a). A fine-grained inner layer in contact with the unreacted core of calcite and an outer rim with coarse crystals are visible in sections after 1 h of reaction, both of them highly porous. As before, both layers were found to be $CaSO_4$ by EDX. Again differences in BSE contrast are likely to be related to differences in porosity, as the Raman spectra from both layers are similar (green spectra in Fig. 7c, d) and similar to that of bassanite. After 24 h of reaction, the replacement rim is thicker (ca. 130 μm) and formed by a mix of fine and coarse $CaSO_4$ crystals (Figs. 4, 7b). The Raman spectra of the replacement rim do not show significant differences regardless of the position analysed, and it is different to that found at $t = 1$hour (red spectra in Fig. 7c, d). In this case, the features of the Raman spectra indicate that anhydrite forms

at this temperature. With increasing reaction time, coarsening of the fine-grained texture and an apparent decrease in porosity are observed (Fig. 4c, d). The Raman spectra of the replacement rim do not vary for $t \geqslant 24$ h.

4. DISCUSSION

4.1. Mineralogical pathway during the $CaCO_3$ to $CaSO_4$ transformation

Microscopic features of partially reacted crystals suggest that during the interaction of calcite with sulphate-bearing acidic solutions, calcite is pseudomorphically replaced by gypsum (22 °C and 60 °C) and anhydrite (120 °C and 200 °C) (Fig. 1). Note that preservation of shape and volume during the $CaCO_3$–$CaSO_4$ transformation in natural samples has long been known (Schiavon,1992; Vergés-Belmin,1994; Rettger, 1926). Despite the fact that metastable intermediate phases (both amorphous and crystalline) are common during calcium sulphate precipitation (e.g. Van Driessche et al., 2012; Wang and Meldrum, 2012; Ossorio et al., 2014), gypsum was the only phase detected in our system at 22 °C and 60 °C using XRD and microRaman spectroscopy. Moreover, at 60 °C gypsum also forms despite the fact that anhydrite is the thermodynamically stable phase. No other phases, particularly bassanite, were detected in our system, despite the fact that this phase has been shown to form at room temperature as a precursor to gypsum precipitation from solutions below its predicted solubility (Van Driessche et al., 2012). Gypsum is known to precipitate homogeneously from solution in the initial stages of the reaction at temperatures as high as 90 °C (Ostroff, 1964) and 120 °C (Ossorio et al., 2014). Its formation in our system ("by-passing" the formation of bassanite) could be possibly influenced by the presence of the calcite substrate. The occurrence of a foreign body (i.e. a substrate) is known to lower the energy barrier for nucleation. When strong interactions and perfect structural match exist between the precipitating phase and the substrate (i.e. a high degree of epitaxy), the nucleation barrier almost vanishes (Liu, 2001). Gypsum shows a better structural match with calcite than bassanite (Ruiz-Agudo et al., submitted). Thus the net effect will be similar to a reduction in the surface energy of the precipitating phase. On the contrary, when the interaction and structural match between the precipitating phase and the substrate is poor, the presence of a substrate has a limited effect on nucleation and thus nucleation will be governed by the homogeneous nucleation kinetics (Liu, 2001).

Although at 120 and 200 °C anhydrite is the thermodynamically stable phase, gypsum and bassanite form first, acting as precursor phases for anhydrite formation. Again, this occurs despite the fact that most of the bulk solutions after the reactions are undersaturated with respect to both metastable phases and at 200 °C even with respect to anhydrite, the final phase formed. The formation of anhydrite as a primary phase within its stability field is thermodynamically and kinetically hampered (Ossorio et al., 2014). First, the larger effective surface free energy for anhydrite compared to that of bassanite and gypsum leads to much longer induction times (i.e. the time for a critical nucleus to form and to be detected) in the case of the former phase (Ossorio et al., 2014). Additionally, anhydrite presents slower growth kinetics than gypsum and, on top of that, two-dimensional nucleation is not an effective growth mechanism on anhydrite and screw dislocations are the main source of steps. This growth mechanism presents structure-induced self-inhibition and thus the growth of anhydrite is inhibited except when a high density of spiral dislocations is present on the surfaces (Morales et al., 2012a, b). Overall, this means that even if a stable anhydrite nucleus is formed in solution, it will take a significant amount of time for it to be detectable (Ossorio et al., 2014). As stated above, precursor phases are frequent during calcium sulphate precipitation, and in particular bassanite is known to occur as an important metastable phase, and its field of apparent stability increases significantly with increasing salinity (Ossorio et al., 2014). At the two highest temperatures studied the mineralogical pathways for the calcite-anhydrite replacement are slightly different. At 120 °C, gypsum and bassanite have similar solubility, and are both metastable with respect to anhydrite. Considering that stability trends are related to surface enthalpy or energy (Navrotsky, 2004), at this temperature both phases should have similar surface energies and, according to the Ostwald step rule, would have the same probability to precipitate from free solutions. However, in our experiments gypsum is the first phase to form. This occurs exclusively in the initial stages of the reaction, and once a first layer of gypsum is formed, further replacement towards the core of the calcite substrate continues in the form of bassanite most likely due to the lower availability of water in the inner region, and coexistence of gypsum and bassanite (below the initially formed gypsum crust) is observed at $t = 1$ h. Subsequently, the thin outer layer of gypsum transforms to bassanite (most likely by dissolution–precipitation, starting from the surface in contact with the fluid). This phase also represents an intermediate stage as it is unstable with respect to anhydrite, and ultimately transforms into the thermodynamically stable phase. Again this occurs most likely by a dissolution precipitation process that it is initiated at the surface in contact with the fluid and progresses towards the core of the sample.

At high salinity, gypsum is not detected at $t = 1$ h. This is not unexpected, as it has been shown that the gypsum to anhydrite transition is facilitated by increasing salinity, and in fact the temperature for gypsum to anhydrite transition is lowered with increasing salinity (Ostroff, 1964; Ossorio et al., 2014). This could be related with the effect of background electrolytes on the hydration shell of calcium, which may assist desolvation of the cation and thus would potentially favour the nucleation of a less hydrated phase (e.g. Kowacz & Putnis, 2008; Ruiz-Agudo et al. 2010, 2011). As well, the lower water activity in the high salinity solution may have favoured the formation of the less hydrated phase.

At 200 °C, gypsum does not form at $t \geqslant 1$ h. Already at $t = 1$ h, a rim formed by an inner layer of fine grained bassanite and an outer layer of coarse grained bassanite are

observed (identified by Raman analysis and GIAXRD). At this temperature, the solubility of gypsum is much higher than that of bassanite, i.e. gypsum is more metastable than bassanite. Both phases are metastable at this temperature and anhydrite is the stable phase. Again, despite being metastable, bassanite forms as a precursor to anhydrite at $t < 24$ h, and ultimately transforms into the stable anhydrite.

4.2. True and partial-equilibrium end points in the replacement of calcite by calcium sulphates

This work shows that, at acidic pH, the interaction of dissolved sulphate with Iceland spar fragments results in the precipitation of calcium sulphates on calcite surfaces. This process involves the release of Ca^{2+} and CO_3^{2-} ions from the calcite surfaces to the solution and the subsequent reaction of Ca^{2+} ions with dissolved SO_4^{2-} to form $CaSO_4$ on dissolving calcite surfaces, leading to the formation of pseudomorphs. Thus the reaction can be described as an interface-coupled dissolution precipitation mechanism. A diffusion-limited growth process is expected due to the reduction in the supply of Ca^{2+} ions from calcite surfaces as a result of the almost complete coverage of the reacting surface by the precipitation of the calcium sulphate phase. Under the different experimental conditions tested, the process stops at a "partial-equilibrium" (Astilleros et al., 2006) end point in which the unreacted calcite become completely isolated from the sulfate-bearing aqueous solution by a dense rim of calcium sulfate crystals and the growth rate of the product layer virtually drops to zero. The complex dependence of the solution chemistry on temperature and salinity reflects the effect of both parameters on calcite and gypsum or anhydrite solubility, as well as the effect of changes in exposed, reactive calcite area as a result of calcium sulfate precipitation.

An increase in temperature during the calcite to anhydrite transformation (120 and 200 °C) results in less calcium available for anhydrite precipitation due to the decrease in calcite solubility, but more anhydrite should precipitate as it is less soluble at higher temperatures. Overall, these effects seem to balance each other and the amount of anhydrite precipitated, and of sulphate removed from the solution, does not vary significantly at these two temperatures. This is in agreement with measurements of the rim thickness growth (Fig. 10), which is not significantly retarded or accelerated with increasing reaction temperature. At higher salinities the solubility of both calcite and anhydrite is higher. But more calcite dissolved results in more calcium available for anhydrite precipitation, so in principle these two effects are opposite and explain why no significant differences are found in the solution chemistry with increasing salinity.

However, higher temperatures seem to promote the replacement of calcite by gypsum (i.e. more calcite is dissolved and more gypsum precipitates with increasing temperature from 22 °C to 60 °C), despite the fact that increasing temperature results in a decrease in calcite solubility and gypsum solubility is not significantly modified in this temperature range. Initially, such an effect would result in less calcium available for gypsum precipitation and a smaller area of the calcite surface covered by the product. This will establish a feedback loop in which the calcite surface area exposed to the solution will be higher and thus more calcium will be available for gypsum precipitation. The net effect seems to be the observed increase in DIC concentration and decrease in sulphate concentration with increasing temperature from 22 °C to 60 °C. This means that at these conditions surface coverage effects overcome solubility effects, and in fact, passivation of the surface seems to be achieved faster at higher temperature (Fig. 10). Interestingly, an increase in salinity at 60 °C results in less calcite dissolved and less gypsum precipitated, which may be as well a result of surface coverage effects. At 22 °C, these effects are apparently less important as more calcite seems to be dissolved and more gypsum precipitated.

As mentioned above, the precipitation of calcium sulphates occurs despite the fact that most of the bulk solutions after the reactions are undersaturated with respect to the precipitating phase(s) (according to our experimental measurements of bulk pH, Ca and S concentrations). To try to explain such observation, simulations of the solution composition during the replacement was performed using the geochemical code PHREEQC (Parkhurst & Appelo, 1999).

First, we assumed that an initial crystal such as those used in our experiments ($4 \times 3 \times 1$ mm, 0.03264 g) reacts in part or completely with 1.5 mL of 100 mM H_2SO_4 solution and the replacement product is in equilibrium with the bulk solution. Such a simulation would represent the "true equilibrium" end point of the system. Table 3 shows pH, Ca, S, and C concentrations calculated at different temperatures and salinities, assuming that gypsum precipitates at 22 °C and 60 °C and anhydrite at 120 °C and 200 °C, respectively. These simulations show that, at the

Table 3
Theoretical composition and saturation indexes with respect to calcium sulfate phases of a 100 mM H_2SO_4 solution at the equilibrium with respect to calcite and gypsum (22 and 60 °C) and anhydrite (120 and 200 °C). Calculations performed using the PHREEQC code.

NaCl 0 M	*T* (°C)			
	22	60	120	200
SI (Gypsum)	0.00	0.00	−0.63	−1.15
SI (Bassanite)	−0.85	−0.39	−0.66	−0.69
SI (Anhydrite)	−0.21	0.14	0.00	0.00
pH	5.72	5.40	5.30	5.42
Ca (mM)	25.31	21.43	6.42	1.30
S (mM)	12.96	13.02	2.38	0.28
C (mM)	112.50	108.60	103.90	100.8
NaCl (4 M)				
SI (Gypsum)	0.00	0.00	−0.74	−1.25
SI (Bassanite)	−0.77	−0.41	−0.68	−0.71
SI (Anhydrite)	−0.09	0.26	0.00	0.00
pH	5.49	5.19	5.20	5.47
Ca (mM)	113.20	94.83	30.83	9.23
S (mM)	75.91	77.18	23.19	6.50
C (mM)	137.30	117.60	107.50	102.6

equilibrium with respect to calcite and gypsum or anhydrite, the simulated solutions have significantly higher pH values than those measured in our experiments (between 1 and 3 in all cases), where the equilibrium is apparently reached. Moreover, sulfate concentrations expected from these calculations are lower than those determined experimentally, while DIC concentrations are higher. As well, in the case of high salinity conditions, the simulated solution composition differs significantly from that measured experimentally.

4.3. Reaction mechanism and molar volume changes

The results of the simulation described above suggest that a mechanism whereby the parent solid reacts in part or completely with the fluid phase and the product is in equilibrium with the bulk solution may not adequately describe the replacement pathway and the equilibrium end-point reached by our system. First, the simulation described above does not consider that, as a result of the precipitation of the newly formed phase, full coverage of the unreacted substrate and blockage of the reaction may occur. Moreover, the assumption of constant composition within the reacting solution during the replacement process is likely to be an oversimplification (e.g. Putnis et al., 2005; Ruiz-Agudo et al., 2012). As shown previously using real-time phase shift interferometry, steep compositional gradients develop at the reacting interface during replacement reactions (Putnis et al., 2005). Therefore, the measured bulk composition may not represent the actual composition of the interfacial fluid (from now on referred to as "boundary layer") from which the replacement product is precipitating. Thus, a more realistic scenario for the replacement reaction may be the dissolution of a small amount of solid in a thin layer of fluid from which the product phase would eventually precipitate, as in Pollok et al. (2011). PHREEQC allows also the calculation of the solution composition in this case, as well the estimation of the amount of precipitated calcium sulphate and thus determination of the volume change during the course of the replacement reaction ($\Delta V_{\text{reaction}}$). This can be calculated as (e.g. Pollok et al. (2011)):

$$\Delta V_{\text{reaction}} = 100 \cdot \left(\frac{n_p \cdot V_{M,p} - n_d \cdot V_{M,d}}{n_d \cdot V_{M,d}} \right) \quad (2)$$

where n_d is the number of moles of calcite dissolved, n_p is the number of moles precipitated, $V_{M,d}$ is the molar volume of calcite (36.9 $cm^3\ mol^{-1}$) and $V_{M,p}$ is the molar volume of gypsum (74.4 $cm^3\ mol^{-1}$), bassanite (53.8 $cm^3\ mol^{-1}$) or anhydrite (46.1 $cm^3\ mol^{-1}$).

To illustrate this in our system, we will assume that a calcite monolayer (0.3 nm thick) dissolves in a solution layer of defined thickness. The dissolution of a 0.3 nm layer of $CaCO_3$ from a 4 × 3 × 1 mm Iceland Spar crystal will lead to a dissolved volume of $CaCO_3$ of 7.8×10^{-9} cm^3, which is equivalent to 2.12×10^{-10} mol $CaCO_3$. If this amount of solid dissolves into a 1 nm thick solution layer of 100 mM H_2SO_4 (22 °C, solution volume of 2.6×10^{-8} cm^3), this solution becomes supersaturated with respect to gypsum (SI = 0.96), bassanite (SI = 0.34) and anhydrite (SI = 0.89). Assuming that gypsum precipitates until SI = 0, then 2.30×10^{-11} mol of gypsum are formed and the reaction occurs in this step with a negative volume change of the reaction (−98%) despite the fact that gypsum has a higher molar volume than calcite; thus, porosity will be generated.

However, when a calcite monolayer dissolves in a 100 nm thick solution layer of the same solution (2.6×10^{-6} cm^3), using a similar calculation a positive

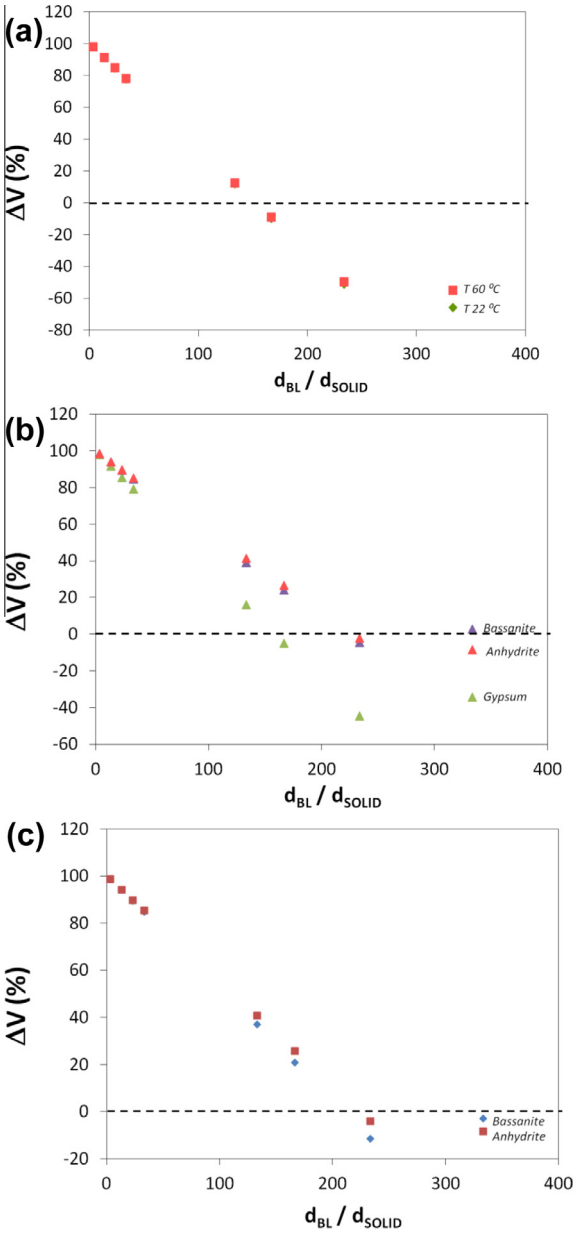

Fig. 11. Volume change (ΔV) during the $CaCO_3$ to $CaSO_4$ transformation as a function of the ratio of the thickness of the fluid layer to the dissolved solid, simulated using PHREEQC code. (a) Low temperature (22 and 60 °C), assuming gypsum precipitation. (b) T 120 °C, assuming gypsum, bassanite or anhydrite precipitation. (c) T 200 °C, assuming bassanite or anhydrite precipitation.

volume change of the reaction (66%) is obtained and porosity is not expected to be generated (based exclusively on relative solubility and molar volume differences). The volume change can be calculated for various ratios of thickness of the solution layer to thickness of dissolved layer and different temperatures, as shown in Fig. 11, assuming precipitation until equilibrium with respect to gypsum, bassanite and/or anhydrite. This simple calculation highlights the importance of the transport and reaction kinetics (that ultimately will determine the thickness of the interfacial layer in which supersaturation with respect to the reaction product is generated) on the porosity developed during replacement reactions.

For a 1000 nm thick solution layer (2.6×10^{-5} cm^3), dissolution of one monolayer of calcite does not result in supersaturation with respect to any $CaSO_4$ phase at any of the temperatures used in our experiments. However, calcite will continue to dissolve and, as a result, the solution composition will evolve and the solution may become supersaturated with respect to a calcium sulfate phase. We will illustrate this in our system for the case of the reactions performed at $T = 120$ °C. In this case, we performed multiple iterative simulations to determine the evolution of the solution composition; in each of these steps, after the dissolution of a calcite monolayer the resulting interfacial solution mixes with the bulk (which modifies its composition). If, as a result of the dissolution steps, the solution at the interface becomes supersaturated with respect to gypsum (which was found by XRD and microRaman analysis to be the first $CaSO_4$ phase formed at 120 °C), this phase is allowed to precipitate until equilibrium is reached. Fig. 12 shows the evolution of pH, saturation index and solution composition of both the bulk solution and the interfacial layer. After the dissolution of ca. 1.9×10^5 monolayers of calcite, the solution at the interface becomes saturated with respect to gypsum, while the bulk solution is still undersaturated. Moreover, once this point is reached, we can calculate the volume of gypsum precipitated in each of these simulations, and thus estimate the local volume change in each of these infinitesimal steps (Table 4). We found out that, after a couple of monolayers are dissolved, ΔV becomes positive, which can result in the passivation of the surface and the eventual blockage of the reaction. Note that, at this point, the bulk solution would be still undersaturated with respect to any $CaSO_4$ phase, in agreement with our experimental measurements (i.e. gypsum precipitation from an interfacial fluid layer despite the fact that the bulk solution is undersaturated). Nevertheless, at this point simulated DIC and sulfate concentrations are lower and higher than those measured in our system. This indicates that the actual amount of calcite dissolved (or gypsum precipitated) for passivation to occur may not be adequately determined in this calculation. Other factors such as the growth mechanism, which determined the way that the volume of product is distributed on the reacting solid, or the formation of reaction-induced fractures, may as well play a role.

Although this calculation is still a simplification, the conclusions obtained are very likely to be valid in our system, as successive simulation steps lead to bulk solution compositions and pH very close to those measured at $t = 1$ h (Fig. 12 and Table 4). The different phase transitions occurring at $T = 120$ °C and 200 °C in the replacement product introduce another level of complexity in the system.

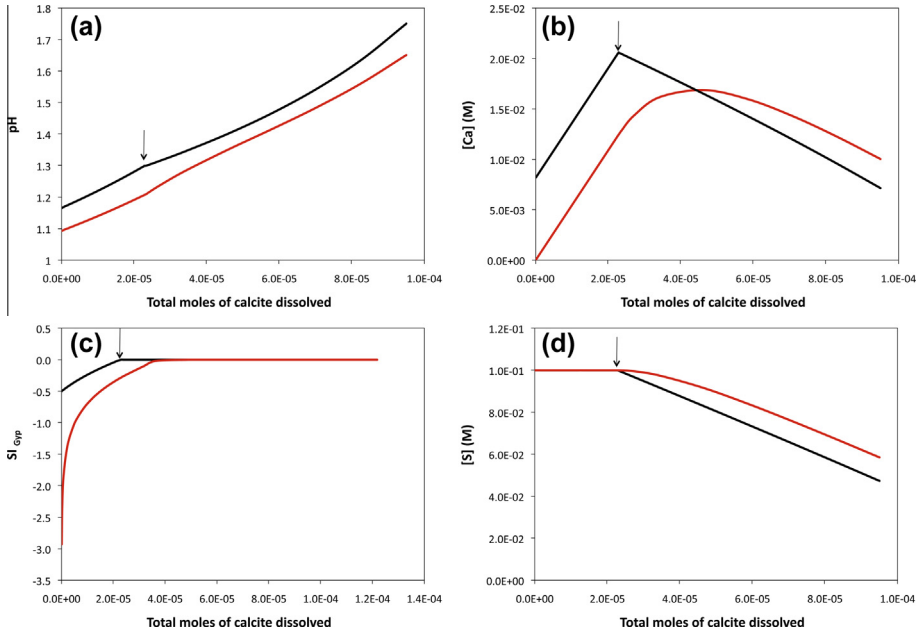

Fig. 12. Evolution of the chemical composition, pH and saturation index with respect to gypsum of the bulk solution and an interfacial fluid layer of thickness 1000 nm during the reaction of calcite (one step = 2.6×10^{-10} mol) with a 100 mM H_2SO_4 solution (initial pH = 1.00) at 120 °C as a function of the amount of calcite dissolved, simulated using the PHREEQC code. The arrow indicates the point at which supersaturation with respect to gypsum is achieved in the 1000 nm solution layer in contact with the solid. Note that the bulk solution still remains undersaturated.

Table 4
Evolution of the composition of the bulk solution and an interfacial fluid layer of thickness 1000 nm during the reaction of calcite with a 100 mM H_2SO_4 solution (initial pH = 1.00) at 120 °C, simulated using the PHREEQC code. The theoretical amount of gypsum precipitated and the volume changes during the reaction are also reported. The simulation was performed in steps, each of them corresponding to the dissolution of a calcite monolayer, i.e. 2.6×10^{-10} mol.

Total calcite dissolved (moles)	Bulk solution					Interfacial solution					Gypsum precipitated in each step (moles)	ΔV (%)
	pH	Ca	C	S	$SI_{Calcite}$	SI_{Gypsum}	pH	Ca	C	S	$SI_{Calcite}$	SI_{Gypsum}		
5.05E−05	1.39	0.0274	0.0275	0.1000	−8.20	−0.20	1.52	0.0351	0.0356	0.0994	−7.73	0	1.43E−11	−89
5.39E−05	1.42	0.0289	0.0293	0.0996	−8.10	−0.16	1.53	0.0345	0.0375	0.0970	−7.69	0	6.80E−11	−47
6.09E−05	1.46	0.0308	0.0331	0.0976	−7.93	−0.10	1.56	0.0333	0.0413	0.0920	−7.59	0	1.47E−10	14
7.31E−05	1.53	0.0315	0.0398	0.0917	−7.69	−0.05	1.62	0.0311	0.0479	0.0832	−7.43	0	2.22E−10	72
8.53E−05	1.60	0.0306	0.0464	0.0842	−7.49	−0.02	1.69	0.0289	0.0546	0.0744	−7.25	0	2.56E−10	99
9.75E−05	1.67	0.0289	0.0530	0.0759	−7.31	−0.01	1.76	0.0266	0.0612	0.0655	−7.07	0	2.73E−10	112
1.10E−04	1.74	0.0269	0.0597	0.0673	−7.12	−0.01	1.85	0.0242	0.0679	0.0565	−6.86	0	2.81E−10	118
1.22E−04	1.83	0.0246	0.0663	0.0584	−6.92	0.00	1.97	0.0218	0.0745	0.0474	−6.62	0	2.87E−10	123

Note that, although the initial precipitation of metastable phases such as gypsum or bassanite may have resulted in the temporal blocking of the reacting surface, its subsequent transformation into anhydrite could have opened new pore space in the replacement rim, as anhydrite is less soluble and has a lower molar volume than both metastable phases. Once anhydrite has nucleated and grown, replacing the precursor phase, progress of the reaction would be by the precipitation of new anhydrite, resulting again in positive volume changes, which would eventually block or hamper the reaction. Future work to determine porosity in the replacement rim at different reaction times (e.g. by microtomography) will be needed to confirm these hypotheses.

5. CONCLUSION

The replacement of calcite by calcium sulphates (gypsum and anhydrite, depending on the reaction temperature) in contact with acidic sulphate bearing solutions most likely occurs via an interface-coupled dissolution–precipitation reaction, in which the substrate is replaced pseudomorphically by the product. At 120 °C and 200 °C, gypsum and bassanite form prior to the thermodynamically stable anhydrite, while at lower temperatures (22 °C and 60 °C) gypsum is the only phase formed. This reaction occurs despite the fact that most of the bulk solutions after the reaction are undersaturated with respect to the precipitating phase(s). This can be understood considering a mechanism for the replacement based on the dissolution of a thin solid layer in a thin layer of fluid, from which the product precipitates. Our PHREEQC simulations confirm that gypsum may precipitate from a thin fluid layer while the bulk fluid remains undersaturated. Moreover, the reaction occurs ultimately with a positive volume change, which eventually results in passivation of the unreacted calcite substrate and explains the fact that the system reaches a "partial" equilibrium point before calcite attains equilibrium with respect to the bulk solution. Simulations of the reaction mechanism also highlight the relevance of transport and surface reaction kinetics on the porosity developed during replacement reactions. Finally, the effect of temperature and salinity on the chemistry of the solutions is a complex interplay between the effect of such parameters on the solubility of the different phases involved and the effect of surface coverage by the precipitating phase. During the calcite to gypsum transformation, temperature and salinity seem to enhance the replacement, while no significant effect is observed in the case of the calcite to anhydrite transformation. Furthermore, salinity tends to promote the formation of less hydrated precursor phases.

ACKNOWLEDGEMENTS

This research was done within the grants MAT2012-37584 and P11-RNM-7550, funded by the Spanish Government, European Commission and the Junta de Andalucía. ER-A acknowledges the receipt of a Ramón y Cajal grant from the Spanish Government (Ministerio de Economia y Competitividad) and funding from the research group RNM-179 of the Junta de Andalucía. The research at Münster is funded by the DFG. The

authors thank Veronika Rapelius for help with the ICP-OES analyses.

REFERENCES

Ahr W. M. (2008) *Geology of carbonate reservoirs: the identification, description and characterization of hydrocarbon reservoirs in carbonate rocks*. John Wiley & Sons Inc.

Astilleros J. M., Pina C. M., Fernández-Díaz L., Prieto M. and Putnis A. (2006) Nanoscale phenomena during the growth of solid solutions on calcite {10$\bar{1}$4} surfaces. *Chem. Geol.* **225**, 322–335.

Atanassova R., Cama J., Soler J. M., Offeddu F. G. and Queralt I. (2013) Calcite interaction with acidic sulphate solutions: a vertical scanning interferometry and energy-dispersive XRF study. *Eur. J. Mineral.* **25**, 331–351.

Booth J., Hong Q., Crompton R. G., Prout K. and Payne R. M. (1997) Gypsum overgrowths passivate calcite to acid attack. *J. Colloid Interface Sci.* **192**, 207–214.

Chio C. H., Sharma S. K. and Muenow D. W. (2004) Micro-Raman studies of gypsum in the temperature range between 9 K and 373 K. *Am. Mineral.* **89**, 390–395.

Cravotta C. A. (2003) Size and performance of anoxic limestone drains to neutralize acidic mine drainage. *J. Environ. Qual.* **32**, 1277–1289.

Cravotta C. A. and Trahan M. K. (1999) Limestone drains to increase pH and remove dissolved metals from acidic mine drainage. *Appl. Geochem.* **14**, 581–606.

Del Monte M. and Sabbioni C. (1984) Gypsum crusts and fly ash particles on carbonate outcrops. *Arch. Meteorol. Geophys. B* **35**, 105–111.

Fernández-Díaz L., Fernandez-Gonzalez A., Carneiro J. and Prieto M. (2009a) On the interaction between gypsum and carbonate-bearing aqueous solutions: implications for the polymorphism of $CaCO_3$. *Geochim. Cosmochim. Acta* **73**. A367-A367.

Fernández-Díaz L., Pina C. M., Astilleros J. M. and Sánchez-Pastor N. (2009b) The carbonatation of gypsum: pathways and pseudomorph formation. *Am. Mineral.* **94**, 1223–1234.

Flörke W. and Flörke O. W. (1961) Vateritbildung aus gips in sodalösung. *Neues. Jb. Miner. Monat.*, 179–181.

García-Rios M., Dávila G., Offeddu F. G., Soler J. M. and Cama J. (2011) Reactions during CO_2 geological sequestration: dissolution of calcite and dolomite coupled to gypsum precipitation. *Macla* **15**, 93–94.

Hardie L. A. (1967) The gypsum-anhydrite equilibrium at one atmosphere pressure. *Am. Mineral.* **52**, 171–200.

Hedin R. S., Watzlaf G. R. and Nairn R. W. (1994) Passive treatment of acid mine drainage with limestone. *J. Environ. Qual.* **23**, 1338–1345.

Hu G., Dam-Johansen K. and Wedel S. (2008) Oriented nucleation and growth of anhydrite during direct sulfation of limestone. *Cryst. Growth Design* **8**, 1081–1085.

Huminicki D. M. C. and Rimstidt J. D. (2008) Neutralization of sulfuric acid solutions by calcite dissolution and the application to anoxic limestone drain design. *Appl. Geochem.* **23**, 148–165.

Johnson D. B. and Hallberg K. B. (2005) Acid mine drainage remediation options: a review. *Sci. Total Environ.* **338**, 3–14.

Kleinmann R. L. P., Hedin R. S. and Nairn R. W. (1998) Treatment of mine drainage by anoxic limestone drains and constructed wetlands. In *Acidic Mining Lakes*. Springer, Berlin, Germany, pp. 303–319.

Kowacz M. and Putnis A. (2008) The effect of specific background electrolytes on water structure and solute hydration: consequences for crystal dissolution and growth. *Geochim. Cosmochim. Acta* **72**, 4476–4487.

Liu X. Y. (2001) Interfacial effect of molecules on nucleation kinetics. *J. Phys. Chem. B* **105**, 11550–11558.

Mazzullo S. J. and Chillingarian G. V. (1992) Diagenesis and origin of porosity. In *Carbonate Reservoir Characterization: A Geologic Engineering Analysis. Developments of Petroleum Science*, 30, pp. 199–270. Carbonate Reservoir Characterization: A Geologic Engineering Analysis. Developments of Petroleum Science. Elsevier Publ. Co.,, Amsterdam.

Morales J., Astilleros J. M. and Fernández-Díaz L. (2012a) Nanoscopic characteristics of anhydrite (100) growth. *Cryst. Growth Design* **12**, 414–421.

Morales J., Astilleros J. M. and Fernández-Díaz L. (2012b) A nanoscopic approach to the kinetics of anhydrite (100) surface growth in the range of temperatures between 60 and 120 °C. *Am. Mineral.* **97**, 995–998.

Murray R. C. (1964) Origin and diagenesis of gypsum and anhydrite. *J. Sediment. Petrol.* **34**, 512–523.

Navrotsky A. (2004) Energetic clues to pathways to biomineralization: precursors, clusters, and nanoparticles. *Proc. Natl. Acad. Sci. U.S.A.* **101**, 12096.

Offeddu F. G., Cama J., Soler J. M. and Putnis C. V. (2014) Direct nanoscale observations of the coupled dissolution of calcite and dolomite and the precipitation of gypsum. *Beilstein J. Nanotechnol.* **5**, 1245–1253.

Ossorio M., Van Driessche A. E. S., Pérez P. and García-Ruiz J. M. (2014) The gypsum–anhydrite paradox revisited. *Chem. Geol.* **386**, 16–21.

Ostroff A. G. (1964) Conversion of gypsum to anhydrite in aqueous solutions. *Geochim. Cosmochim. Acta* **28**, 1361–1372.

Parkhurst D. L. and Appelo C. A. J. (1999) Users guide to PHREEQC (version 2) – a computer program for speciation, batch reaction, one dimensional transport, and inverse geochemical calculations. U.S. Geological Survey Water-Resources Investigation Report 99–4259, p. 312.

Pollok K., Putnis C. V. and Putnis A. (2011) Mineral replacement reactions in solid solution-aqueous solution systems: volume changes, reactions paths and end-points using the example of model salt systems. *Am. J. Sci.* **311**, 211–236.

Putnis A. (2002) Mineral replacement reactions: from macroscopic observations to microscopic mechanisms. *Mineral. Mag.* **66**, 689–708.

Putnis A. (2009) Mineral replacement reactions. In thermodynamics and kinetics of water-rock interactions. *Rev. Mineral. Geochem.* **30**, 87–124.

Putnis A. and Putnis C. V. (2007) The mechanism of reequilibration of solids in the presence of a fluid phase. *J. Solid State Chem.* **180**, 1783–1786.

Putnis C. V., Tsukamoto K. and Nishimura Y. (2005) Direct observations of pseudomorphism: compositional and textural evolution at a fluid-solid interface. *Am. Mineral.* **90**, 1909–1912.

Rettger R. E. (1926) Replacement of calcite by gypsum. *Am. Mineral.* **9**, 153.

Roncal-Herrero T., Bots P., Rodríguez-Blanco J. D., Astilleros J. M., Prieto M., Benning L. and Fernández-Díaz L. (2013) Are the anhydrite and gypsum carbonatation pathways the same? *Mineral. Mag.* **77**, 2081.

Ruiz-Agudo E., Kowacz M., Putnis C. V. and Putnis A. (2010) The role of background electrolytes on the kinetics and mechanism of calcite dissolution. *Geochim. Cosmochim. Acta* **74**, 1256–1267.

Ruiz-Agudo E., Putnis C. V., Wang L. and Putnis A. (2011) Specific effects of background electrolytes on the kinetics of step

propagation during calcite growth. *Geochim. Cosmochim. Acta* **75**, 3803–3814.

Ruiz-Agudo E., Putnis C. V., Rodriguez-Navarro C. and Putnis A. (2012) Mechanism of leached layer formation during chemical weathering of silicate minerals. *Geology* **40**, 947–950.

Ruiz-Agudo E., Putnis C. V. and Putnis A. (2014) Coupled dissolution and precipitation at mineral–fluid interfaces. *Chem. Geol.* **383**, 132–146.

Schiavon N. (1992) Decay mechanisms of oolitic limestones in an urban environment: King's College Chapel, Cambridge and St. Luke's Church, London. In: Stone cleaning and the nature, soiling and decay mechanisms of stone: proceedings of the international conference held in Edinburgh, U.K., 14–16 April 1992, Donhead, London (1992), pp. 258–267

Van Driessche A. E. S., Benning L. G., Rodriguez-Blanco J. D., Ossorio M., Bots P. and Garcia-Ruiz J. M. (2012) The role and implications of bassanite as a stable precursor phase to gypsum precipitation. *Science* **336**, 69–72.

Vergés-Belmin V. (1994) Pseudomorphism of gypsum after calcite, a new textural feature accounting for the marble sulphation mechanism. *Atmos. Environ.* **28**, 295–304.

Wang Y.-W. and Meldrum F. C. (2012) Additives stabilize calcium sulfate hemihydrate (bassanite) in solution. *J. Mater. Chem.* **22**, 22055–22062.

Associate editor: Robert H. Byrne